IAC-20,C4,5,11,x58032

RF Helicon-based Plasma Thruster (IPT): Design, Set-up, and First Ignition.

F. Romano[a*], Y.-A. Chan[a] G. Herdrich[a], P. C.E. Roberts[b], C. Traub[a], S. Fasoulas[a], N. Crisp[b], S. Edmondson[b], S. Haigh[b], B. A. Holmes[b], S. Livadiotti[b], A. Macario-Rojas[b], V. T. Abrao Oiko[b], K. Smith[b], L. Sinpetru[b], J. Becedas[c], R. M. Dominguez[c], S. Christensen[d], T. K. Jensen[d], J. Nielsen[d], M. Bisgaard[d], D. Garcia-Almiñana[e], S. Rodriguez-Donaire[e], M. Sureda[e], M. Garcia-Berenguer[e], D. Kataria[f], R. Villain[g], S. Seminari[g], A. Conte[g], B. Belkouchi[g].

[a] *Institute of Space Systems (IRS), University of Stuttgart, Pfaffenwaldring 29, 70569, Germany*
[b] *The University of Manchester, Manchester, George Begg Building, Sackville Street, Manchester, M13 9PL, UK.*
[c] *Elecnor Deimos Satellite Systems, Calle Francia 9, 13500 Puertollano, Spain*
[d] *GomSpace AS, Langagervej 6, 9220 Aalborg East, Denmark*
[e] *UPC-BarcelonaTECH, Carrer de Colom 11, 08222 Terrassa, Barcelona, Spain*
[f] *Mullard Space Science Laboratory (UCL), Holmbury St. Mary, Dorking, RH5 6NT, United Kingdom*
[g] *Euroconsult, 86 Boulevard de Sébastopol, 75003 Paris, France*
*Corresponding Author: romano@irs.uni-stuttgart.de

ABSTRACT

To extend missions lifetime at very low altitudes, an efficient propulsion system is required to compensate for aerodynamic drag. One solution is Atmosphere-Breathing Electric Propulsion (ABEP). It collects atmospheric particles to be used as propellant for an electric thruster. The system ideally nullifies the requirement of onboard propellant storage. An ABEP system can be applied to any celestial body with atmosphere (Mars, Venus, Titan, etc.), enabling new mission at low altitude ranges for longer times. Challenging is operation of the thruster on reactive chemical species, such as atomic oxygen (AO), that is highly present in low Earth orbit, as they cause erosion of (not only) propulsion system components, i.e. acceleration grids, electrodes, neutralizers, and discharge channels of conventional EP systems. For this reason, a contactless plasma thruster is developed: the RF helicon-based plasma thruster (IPT). The paper describes the thruster design, implementation, and first ignition tests. The thruster presents a novel antenna called the birdcage antenna that is implemented for decades in magnetic resonance imaging (MRI) machines. The design is supported by the simulation tool XFdtd®. The IPT is aided by an externally applied static magnetic field that provides the boundary condition for the helicon wave formation within the plasma discharge. The antenna working principle allows to minimize losses in the electric circuit and provides, together with the applied magnetic field, acceleration of a quasi-neutral plasma plume.

Keywords: Atmosphere Breathing Electric Propulsion, Plasma Thruster, Very Low Earth Orbit, Helicon, Birdcage.

Acronyms/Abbreviations

AO:	Atomic Oxygen
ABEP:	Atmosphere-Breathing Electric Propulsion
EP:	Electric Propulsion
IPT:	RF Helicon-based Plasma Thruster
VLEO:	Very Low Earth Orbit
S/C:	Spacecraft

INTRODUCTION

The RF Helicon-based Plasma Thruster (IPT) is designed within the EU H2020 DISCOVERER project [1], that aims to redesign very low Earth orbit (VLEO < 450 km) platforms by researching low drag materials, aerodynamic attitude control, and Atmosphere-Breathing Electric Propulsion (ABEP) see Figure 1.
Orbiting in VLEO can open a new range of space missions [2], however, the mission lifetime is a limiting factor due to aerodynamic drag. To extend it, an efficient propulsion system is required, but the lifetime is then limited by the amount of propellant on board. An ABEP system collects the atmospheric particles in VLEO by an intake and feeds an electric thruster which ionizes and accelerates them to generate thrust. This can counteract the drag and at the same time remove to requirement of carrying propellant on-board. Such system can be applied to any planet with atmosphere given that enough electric power is

provided. Within DISCOVERER an RF contactless thruster, the IPT, is developed. The contactless nature removes any issue of erosion of component in contact with the plasma due to the use of atomic oxygen O as propellant (dominant alongside N_2 in VLEO), as well as it produces a quasi-neutral plasma plume, removing the requirement of a neutralizer working on atmospheric propellant as well. The IPT is based on a birdcage antenna, a device developed decades ago for magnetic resonance imaging (MRI) machines [3]. The design is such to minimize losses in the electric circuit as well as producing a convenient electromagnetic field configuration for quasi-neutral plasma acceleration.

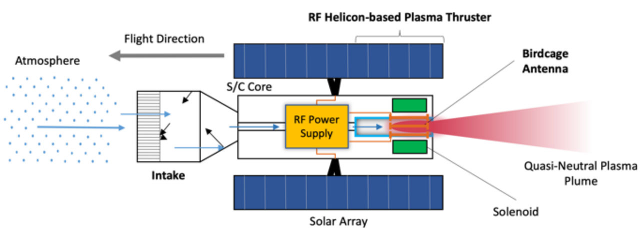

Figure 1 ABEP Concept [4].

RF HELICON-BASED PLASMA THRUSTER (IPT) DESIGN

The requirements set within DISCOVERER are to develop an RF contactless plasma thruster to be operated with variable mixtures of N_2 and atomic oxygen AO as propellant with $P_{in} < 5\,kW$.

The contactless nature of the thruster is crucial to cope with the chemically aggressive AO, one of the main species in VLEO. In conventional EP systems, such as gridded ion and Hall-effect thrusters, erosion of grids and discharge channels will reduce thruster's performance over time rapidly [7,8]. Moreover, the IPT plasma plume is to be quasi-neutral and therefore does not require a neutralizer, another challenging device to design for atmospheric propellant operation [9,10].

The first version of the IPT is a model for laboratory testing, designed for maximum (technical) flexibility to allow for easy modifications for optimization purposes. Following the design of mechanical and vacuum interfaces [9], the crucial element of the IPT design is the antenna and its respective tuning which will be described in the following sections.

RF CIRCUIT DESIGN

According to results from HELIC and ADAMANT presented in [10] a frequency higher than $f = 27.12\,MHz$ is preferable, as it leads to easier ignition, important for ABEP operation, and better power absorption at higher plasma densities when associated with an applied static magnetic field [10,11]. The acquired RF-Generator and auto-matching network operates at $f = 40.68\,MHz$ input frequency, and the IPT discharge channel is of $\phi = 37\,mm$ inner diameter. In general, antenna and plasma are seen in the RF circuit as an equivalent impedance Z, with both real (resistance R) and imaginary (reactance X) components, see Eq.(1) [13].

$$\vec{Z} = \vec{R} + j\vec{X}$$
$$X = X_L + X_C = 2\pi f L + \left(-\frac{1}{2\pi f C}\right) \tag{1}$$

From the thruster electrical point of view, the system as a whole, including the RF generator, its matching network, connectors, and connecting cables must be optimized [14]. In an RF circuit, the power transfer from a source (RF generator) to its load (IPT) is maximized only if the load's impedance Z_L is matched to that of the source Z_S. RF generators industrial standard is of $Z_S = 50 + j0\,\Omega$ purely resistive output. The matching network dynamically creates a resonant circuit with the load, matching it to Z_S by a system of variable inductors and capacitors. This reduces the reflected power reaching the RF generator, but it does not improve the load itself. Finally, an optimum design of the antenna is required to minimize losses. Plasma is a variable impedance that would need a further dynamic fine-tuning control. Within the IPT design, first, an accurate selection of cabling, connectors is done, and second, an optimized antenna is built, the simplified schematics of the IPT RF circuit is shown in Figure 2.

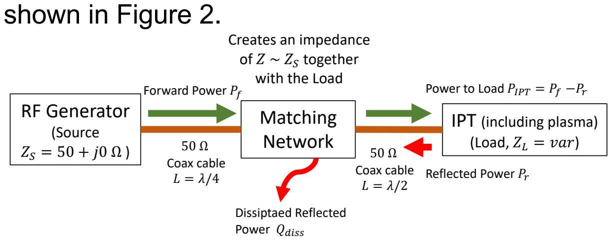

Figure 2 Schematics of IPT RF circuit [4].

THE BIRDCAGE ANTENNA

The birdcage antenna is a device originally developed for Magnetic Resonance Imaging (MRI) [3]. When operated at one of their resonance frequencies, the antenna generates a homogeneous transversal magnetic field that can be either linearly or circularly polarized. Birdcage antennae operate on the principle that a sinusoidal current distribution over a cylindrical surface induces a homogeneous transversal magnetic field within the volume itself. They are made of two end-rings, connected by equally spaced legs. The legs and/or the end-rings have capacitors in between to tune the antenna to the desired the resonance frequency. Birdcage antennae can be designed as low-pass, high-pass, or band-pass frequency response depending on the capacitor locations, see a schematic representation in Figure 3.

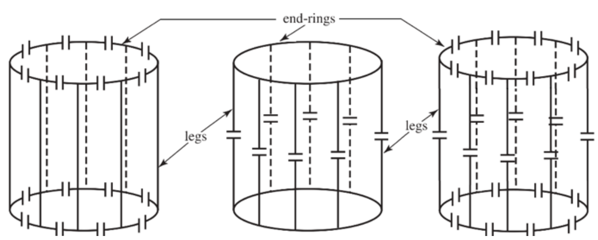

Figure 3 Birdcage Antenna: high-pass (left), low-pass (middle), band-pass (right) (adapted from [15]*).*

Birdcage antennae operate at one of their resonance frequencies, where $X = 0\ \Omega$ and the impedance Z is purely real. In such way, the load is already partially matched and only the resistance needs to be further matched. Moreover, at such condition, the electromagnetic (EM) fields are perpendicular to each other and homogeneous within the cross section of the discharge channel. Depending on the feed, such fields can be linearly or circularly polarized.

Each antenna has $k = N/2$ resonance frequencies. The current distribution along the antenna follows the law described in Eq. (*2*), where $\mathrm{I_{jk}}$ is the normalized current at the j-th loop for the k mode of a birdcage antenna with N legs.

$$I_{jk} = \begin{cases} cos\left(\frac{2\pi jk}{N}\right), & k = 0,1,2,\dots,N/2 \\ \sin\left(\frac{2\pi jk}{N}\right), & k = 1,2,\dots,\left(\frac{N}{2} - 1\right) \end{cases} \quad (2)$$

Therefore, the more legs, the more the current distribution matches a sinusoidal curve, see Figure 4. Birdcage antennas are modeled by self and mutual inductances of legs and end-rings L_{Leg} and L_{ER}, plus the applied capacitors of capacitance C [20,21]. Resonance frequencies for the high pass design are given in Eq. (*3*).

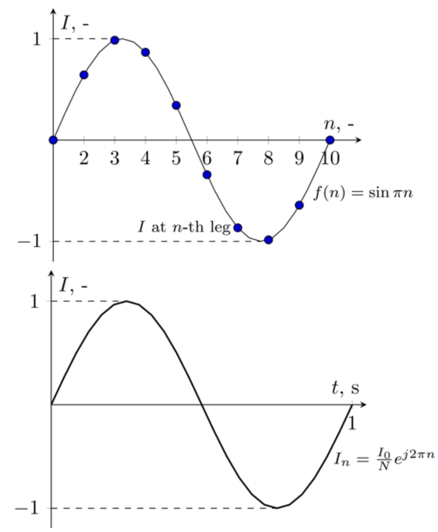

Figure 4 Current distribution along a 10-leg birdcage at a given time (top), current amplitude over time on a single leg (bottom) [4].

The high pass design has one resonance mode more ($k = 0$) at the highest frequency named anti-resonant, AR.

$$\omega_{k_{HP}} = \left[C\left(L_{ER} + 2\, L_{Leg} \sin^2 \frac{\pi k}{N}\right)\right]^{-\frac{1}{2}}$$

$$(k = 0,1,2,\dots,N/2) \quad (3)$$

Only the resonant mode $k = 1$ produces the required homogeneous EM fields configuration.

In terms of EM fields, the magnetic field created by the birdcage, see Figure *5*, is $\vec{B}_1$ along y, the respective electric field $\vec{E}_1$ is perpendicular to $\vec{B}_1$, along x. Since $\vec{B}_1$ is linearly polarized, its direction will switch along y on each cycle, and so will $\vec{E}_1$ along x. An additional external static magnetic field is provided along the z axis, $\vec{B}_0$, to provide the boundary condition for the formation of helicon waves. Indeed, at EPFL helicon plasma are generated for fusion research using birdcage antennae operating at $13.56\ MHz$ for RF powers up to $10\ kW$ [17]–[19].

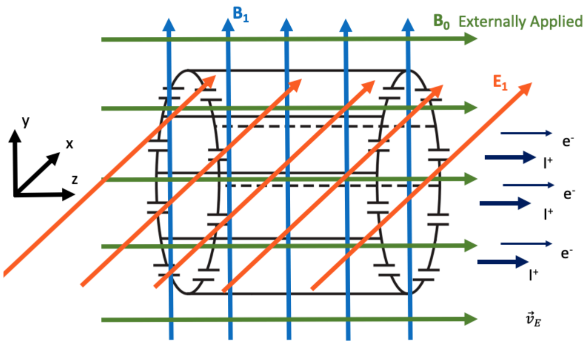

Figure 5 Birdcage EM fields $\boldsymbol{B_1}$, $\boldsymbol{E_1}$, externally applied magnetic field $\boldsymbol{B_0}$ [4].

The resulting EM fields created by the antenna can provides a drift velocity $\vec{v}_E = \vec{E} \times \vec{B}$ imparted to both ions and electrons in the same direction along z. This can provide thrust, together with the magnetic nozzle effect provided by the static applied magnetic field, while producing a quasi-neutral plasma exhaust that does not require a neutralizer, see Eq. (4). Such results support the use of a birdcage antenna for a contactless plasma thruster application.

$$\vec{v}_E = \frac{1}{\vec{B}^2} \left\| \begin{matrix} \hat{x} & \hat{y} & \hat{z} \\ E_1 & 0 & 0 \\ 0 & B_1 & B_0 \end{matrix} \right\| = \frac{1}{{B_0}^2 + {B_1}^2} \begin{Bmatrix} 0 \\ -E_1 B_0 \\ E_1 B_1 \end{Bmatrix} \tag{4}$$

IPT DESIGN, INTEGRATION, AND VERIFICATION

The main components of the IPT are: propellant injector, discharge channel, birdcage antenna, Faraday shield, solenoid, and the support structure, see Figure 6. The injector is movable along the symmetry axis z, it is made of conductive material and used for fine-tuning the thruster. The solenoid is located externally to produce the static magnetic field. It is designed to produce a magnetic field up to $70\,mT$ with $15\,A$ current. At such current, more than $30\,min$ operation is possible without overheating to allow for future plasma diagnostic measurements.

The birdcage antenna has 8 legs in a high pass configuration, designed to resonate at $40.68\,MHz$. The feed is at one point, to provide linearly polarized EM fields. The commercial 3D EM software Remcom Inc. XFdtd® 7.8.1.3 is used to evaluate the resonance spectrum and the corresponding impedances to support the antenna design, especially the choice of the correct capacitance. The IPT structure is made of brass to minimize Eddie currents due to the RF fields, as well as to minimize interactions with the applied static magnetic field. The birdcage antenna is enclosed within a brass Faraday shield that isolates the outer environment from the EM fields created by the antenna and vice versa.

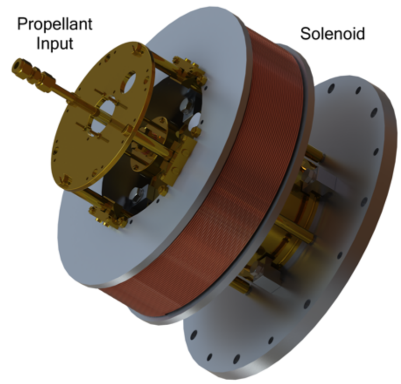

Figure 6 IPT rendering with the external solenoid [4].

The resonance study results with XFdtd® are shown in terms of S_{11} (scattering parameter), and impedance Z in Figure 8 and Figure 9. Each peak of S_{11} is a resonant frequency, correspondingly, $X = 0\,\Omega$. To verify that the $k = 1$ is the correct one, the EM fields are visualized in 3D, see Figure 9, compared to that of the other peaks, and verified to be linearly polarized and homogeneous within the transversal section [20]. At each RF cycle the EM fields reverse their directions. Once the correct resonance peak is identified, the capacitance is swept until the peak is at $40.68\,MHz$, finally requiring a capacitance of $C = 785.51\,pF$. The applied static magnetic field is expected to aid the formation of helicon waves within the discharge channel therefore providing a higher degree of ionization [22,23].

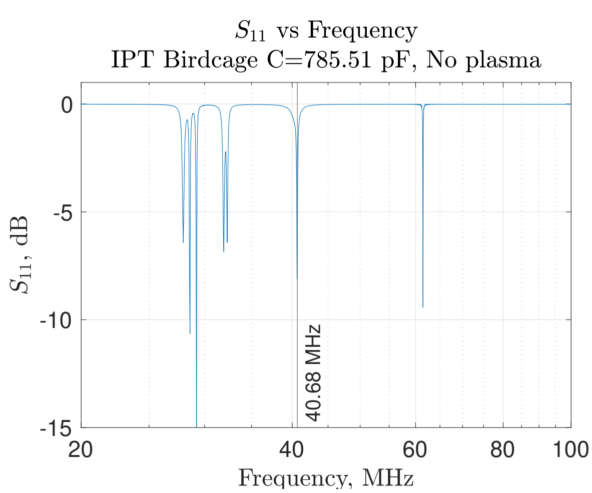

Figure 7 S_{11} vs Frequency IPT, XFdtd® Simulation [4].

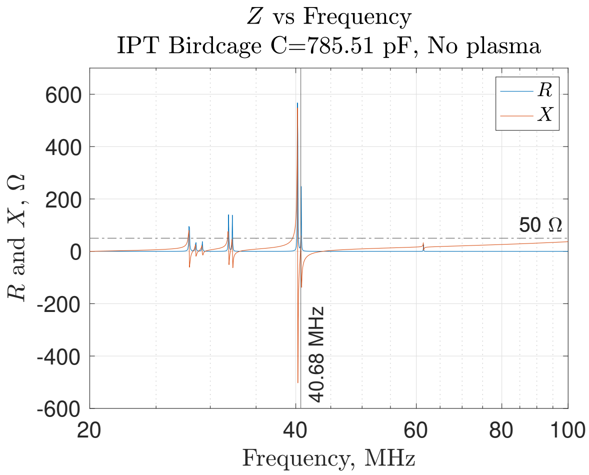

Figure 8 Z vs frequency IPT, XFdtd® Simulation [4].

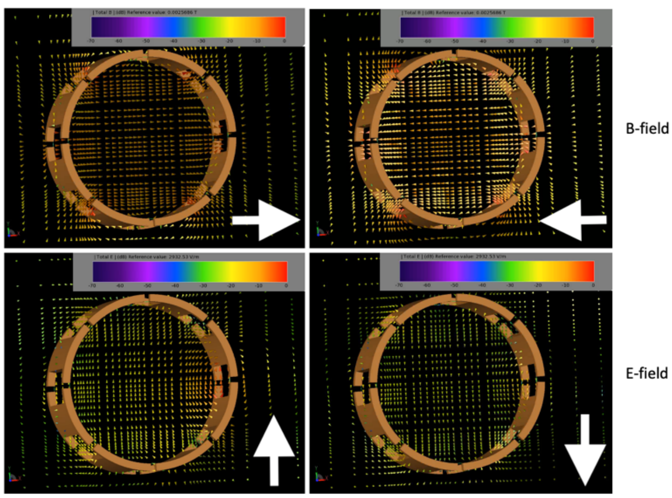

Figure 9 Magnetic Field (top) and Electric Field (bottom): linear polarization [4].

RESONANCE TUNING

The integration of the IPT carries uncertainties and shifts from the desired resonance frequency and impedance due to tolerances in manufacturing, assembly, and non-ideal electrical components, such as the capacitors. Finally, the IPT requires to be further tuned tuning, and finally fine-tuned once everything is in place. While further tuning is achieved in the birdcage antenna integration phase, the fine-tuning is built-in the IPT. This is achieved by the moving conductive injector: it fine-tunes the resonance frequency once the IPT is fully integrated. After ignition, a frequency shift and a corresponding impedance change will still happen, but it is expected to be minimal due to the small size of the discharge channel. The assembled IPT is shown in Figure 10.

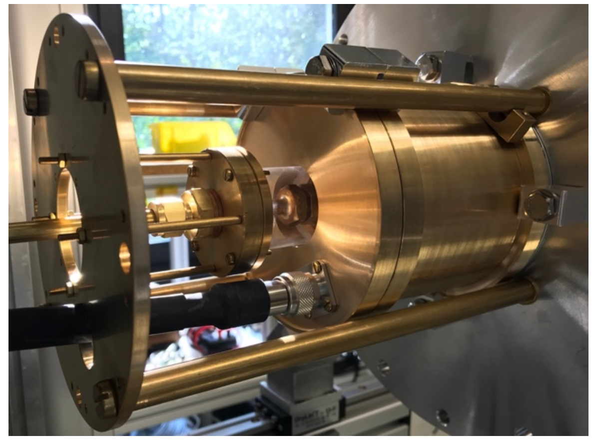

Figure 10 IPT assembled, [20].

TESTING

The assembled IPT is connected to the calibrated NanoVNA v2 network analyser to verify its performance in terms of S_{11} and impedance Z. The final tuning is presented in Figure 11, resulting in an $S_{11} = -24.8\ dB$ corresponding in > 99% of the power coupled in the antenna.

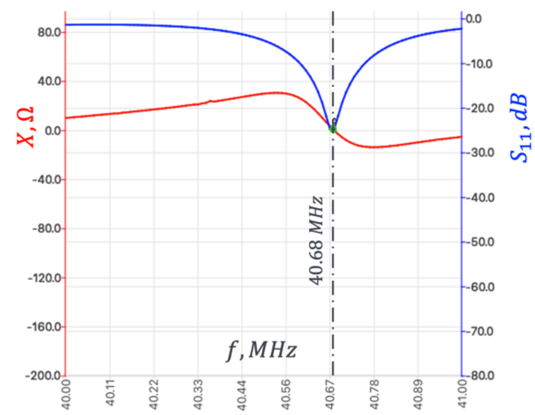

Figure 11 S_{11} and X vs Frequency IPT, measured with a NanoVNA v2.

The first discharge characterization campaign of the IPT has been completed at the end of September 2020. While data are currently being analysed, three exemplary conditions are hereby shown, with the IPT operating on Argon, Nitrogen, and Oxygen, see Figure 12, Figure 13, and Figure 14. All the pictures were taken through a quartz window and with the same camera exposure settings. The input parameters are a forward power $P_f = 60W$, input current for the solenoid $I_S = 6.7A$, a particle flux equal for the three conditions of $20.30\ 1/s$, and a background pressure of $p_{ch} = 0.12 - 0.23\ Pa$.

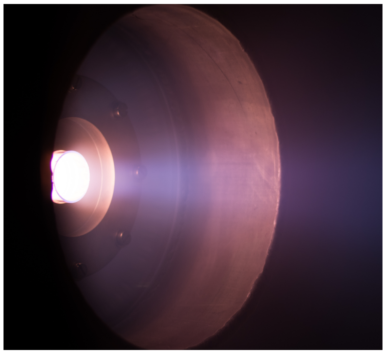

Figure 12 IPT operating on Argon.

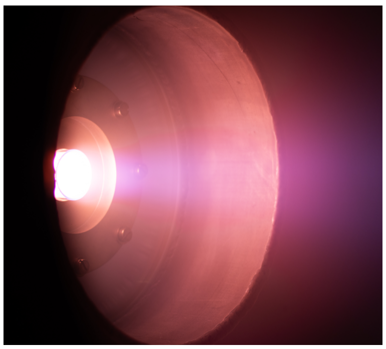

Figure 13 IPT operating on Nitrogen.

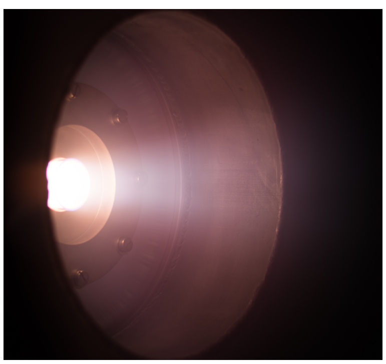

Figure 14 IPT operating on Oxygen.

CONCLUSION

The IPT is a RF contactless plasma thruster based on a birdcage antenna. This has been designed, assembled, and tested. The birdcage antenna operating at resonance ensures a partially matched load by having $X = 0\,\Omega$. Moreover, the EM field configuration produces a drift velocity for ions and electrons towards the same direction resulting in a quasi-neutral plasma plume that does not require a neutralizer. The movable injector is used for fine-tuning the resonance frequency. First ignition has been achieved in March 2020 and the discharge characterization test campaign is in the post-processing phase. The IPT has been tested for different propellants and flows, powers, and magnetic field strengths. The IPT has shown so far easy ignitability, also at very low propellant flow rates, with very low input power required. Further tuning has also been achieved by adjusting the applied magnetic field. To verify the presence of helicon waves within the discharge, B-dot probe measurement will be performed. Moreover, in the near future the plasma will be evaluated by RF compensated plasma diagnostics such as Langmuir and Faraday probes at first, and then using a Retarding Potential Analyser (RPA) and optical emission spectroscopy (OES).

ACKNOWLEDGEMENTS

This project has received funding from the European Union's Horizon 2020 research and innovation programme under grant agreement No. 737183. This reflects only the author's view and the European Commission is not responsible for any use that may be made of the information it contains.

Bibliography

[1] P. C. E. Roberts *et al.*, "DISCOVERER: Developing Technologies to Enable Commercial Satellite Operations in," in *International Astronautical Congress*, 2020.

[2] N. H. Crisp *et al.*, "The Benefits of Very Low Earth Orbit for Earth Observation Missions," *Prog. Aerosp. Sci.*, vol. Accepted, 2020.

[3] C. E. Hayes, W. A. Edelstein, J. F. Schenck, O. M. Mueller, and M. Eash, "An efficient, highly homogeneous radiofrequency coil for whole-body NMR imaging at 1.5 T," *J. Magn. Reson.*, vol. 63, no. 3, pp. 622–628, 1985.

[4] F. Romano *et al.*, "RF helicon-based inductive plasma thruster (IPT) design for an Atmosphere-Breathing Electric Propulsion system (ABEP)," *Acta Astronaut.*, Jul. 2020.

[5] M. Andrenucci, D. Feili, G. Cifali, D. Valentian, T. Misuri, and P. Rossetti, "Preliminary characterization test of HET and RIT with Nitrogen and Oxygen," no. August, pp. 1–16, 2012.

[6] G. Cifali *et al.*, "Completion of HET and RIT characterization with atmospheric propellants," in *3rd Space Propulsion Conference*, Bordeaux, 2012.

[7] T. Andreussi *et al.*, "Development and

Experimental Validation of a Hall Effect Thruster RAM-EP Concept," in *35th International Electric Propulsion Conference*, Atlanta, USA, 377, 2017.

[8] T. Andreussi *et al.*, "Development Status and Way Forward of SITAEL ' s Air-breathing Electric Propulsion," in *AIAA Propulsion and Energy Forum*, Indianapolis, 2019.

[9] F. Romano *et al.*, "Advances on the Inductive Plasma Thruster Design for an Atmosphere-Breathing EP System," *69th Int. Astronaut. Congr. Adelaide, Aust.*, no. IAC-18.C4.6.4x46387, 2018.

[10] S. Masillo *et al.*, "Analysis of electrodeless plasma source enhancement by an externally applied magnetic field for an inductive plasma thruster (IPT).," in *Russian-German Conference on Electric Propulsion*, Rauischholzhausen, RGCEP A079, 2018.

[11] Romano et al, "System Analysis and Test-Bed for an Atmosphere-Breathing Electric Propulsion System Using an Inductive Plasma Thruster," *67th Int. Astronaut. Congr.*, no. September, pp. 25–29, 2017.

[12] F. Romano *et al.*, "Performance Evaluation of a Novel Inductive Atmosphere-Breathing EP System," *35th Int. Electr. Propuls. Conf. Atlanta, USA*, vol. IEPC-2017, no. 184, pp. 1–2, 2017.

[13] D. Melazzi and V. Lancellotti, "ADAMANT: A surface and volume integral-equation solver for the analysis and design of helicon plasma sources," *Comput. Phys. Commun.*, vol. 185, no. 7, pp. 1914–1925, 2014.

[14] A. W. Kieckhafer and M. L. R. Walker, "Rf power system for thrust measurements of a helicon plasma source," *Rev. Sci. Instrum.*, vol. 81, no. 7, pp. 1–8, 2010.

[15] J. Jin, "Electromagnetics in Magnetic Resonance Imaging - IEEE Antennas and Propagation Magazine," *Clin. Imaging*, vol. 40, no. 6, pp. 7–22, 1998.

[16] A. A. Howling, P. Guittienne, R. Jacquier, and I. Furno, "Complex image method for RF antenna-plasma inductive coupling calculation in planar geometry. Part I: Basic concepts," *Plasma Sources Sci. Technol.*, vol. 24, no. 6, 2015.

[17] A. A. Howling, P. Guittienne, C. Hollenstein, and I. Furno, "Resonant rf network antennas for inductively-coupled plasma sources," vol. i, p. 125005, 2014.

[18] I. Furno *et al.*, "A novel helicon plasma source for negative ion beams for fusion," *Nibs*, no. September, 2016.

[19] I. Furno *et al.*, "Helicon wave-generated plasmas for negative ion beams for fusion," *EPJ Web Conf.*, vol. 157, p. 03014, 2017.

[20] F. Romano *et al.*, "Inductive Plasma Thruster (IPT) for an Atmosphere-Breathing Electric Propulsion System: Design and Set in Operation," in *36th International Electric Propulsion Conference*, Vienna, Austria, 2019.

[21] F. F. Chen, "Permanent Magnet Helicon Source for Ion Propulsion," *IEEE Trans. Plasma Sci.*, vol. 36, no. 5, pp. 2095–2110, 2008.

[22] R. Jacquier *et al.*, "First B-dot measurements in the RAID device, an alternative negative ion source for DEMO neutral beams," *Fusion Eng. Des.*, vol. 146, pp. 1140–1144, Sep. 2019.